

Introduction

Snow cover plays a critical role in terrestrial hydrological, climatological, and eco-logical processes. It influences the energy balance on the land surface, based on its high albedo and low thermal conductivity. The measurement of snow water equivalent (SWE) is important to understand the timing and magnitude of snowmelt runoff. Snow density is the key to converting snow depth to snow water equivalent. However, after the snow depth is retrieved, the error in snow density auxiliary information becomes an important source of SWE uncertainty. Snow density varies spatially, temporally, and vertically, influenced by the snow compaction rate and snow compaction time. The use of a fixed snow density (for example, 240 kg/m³) will result in an overestimated snow water equivalent (SWE) in the early snow season and an underestimated SWE in the late snow season. In a warming climate, the direct observation of snow density can be of great value to detect the increased occurrence of rain-on-snow events.

Study Area

The study area is located in Quebec, Eastern Canada (Figure 1). Characterized by cool temperatures in summer and abundant snowfall in winter. Snow in this region has large spatial variability, with a snow cover duration ranging from 120 days in Southern Quebec to 240 days in Northern Quebec, and an annual maximum SWE from less than 100 mm at low altitudes to more than 300 mm at high altitudes.

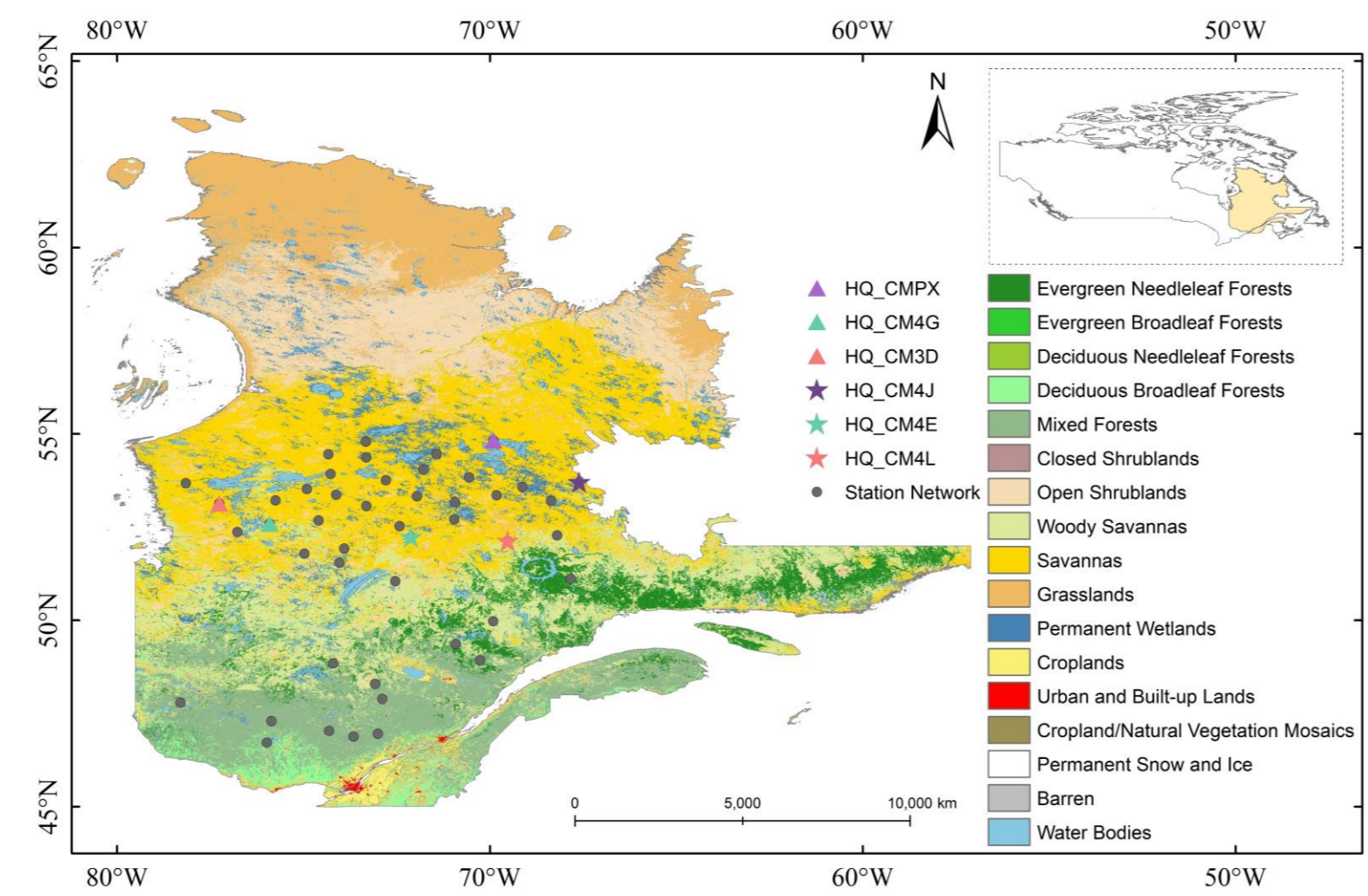


Figure 1. Spatial distribution of stations in Quebec, Canada.

Methods

Forward Emission Model

The radiative transfer model used to describe the emission of the soil–snow–vegetation system is an empirical rough soil reflectivity model, coupled with a simplified snow emission model neglecting absorption and scattering coefficients and a τ - ω vegetation model.

$$T_B^p = T_{B,f}^p F_C + T_{B,S}^p (1 - F_C) \quad (1)$$

$$T_{B,f}^p = T_{B,S}^p \gamma + T_C (1 - \omega) (1 - \gamma) + T_C (1 - \omega) (1 - \gamma) r^p \gamma \quad (2)$$

$$T_{B,S}^p = \frac{(1 - s_G^p)(1 - s_S^p)}{1 - s_G^p s_S^p} \cdot T_G + \frac{s_G^p + s_S^p - 2s_G^p s_S^p}{1 - s_G^p s_S^p} \cdot T_{sky} \quad (3)$$

$$s_G^p = ((1 - Q_R) s_G^{p*} + Q_R \cdot s_G^{q*}) \exp(-H_R \cdot \cos^{N_{RP}} \theta) \quad (4)$$

$$H_R = \left(\frac{a_1 S_D}{a_2 S_D + a_3} \right)^6 \quad (5)$$

- F_C : forest cover fraction
- T_C : soil physical temperature
- T_{sky} : downwelling sky T_B
- s_G^p : snow–soil interface reflectivity
- s_S^p : specular air–snow interface reflectivity
- $Q_R = 0.075$
- $N_{RV} = 1.503$ $N_{RH} = 0.131$
- $a_1 = 0.887$, $a_2 = 0.796$, $a_3 = 3.517$

Retrieval of Predetermined Parameters (τ , ω , S_D) in Snow-Free Period

$$T_{B,error}(\tau, \omega, S_D) = \sum_{t=1}^{t_n} \sum_{\theta_k=0}^{\theta_n} \sum_{p=H,V} (T_{B,obs}^p(\theta_k, t) - T_{B,mod}^p(\theta_k, t, \tau, \omega, S_D))^2 \quad (6)$$

Retrieval of Snow Density

$$CF(\rho_S) = \sum_{\theta_k=0}^{\theta_n} \sum_{p=H,V} (T_{B,obs}^p(\theta_k) - T_{B,mod}^p(\theta_k, \rho_S))^2 \quad (7)$$

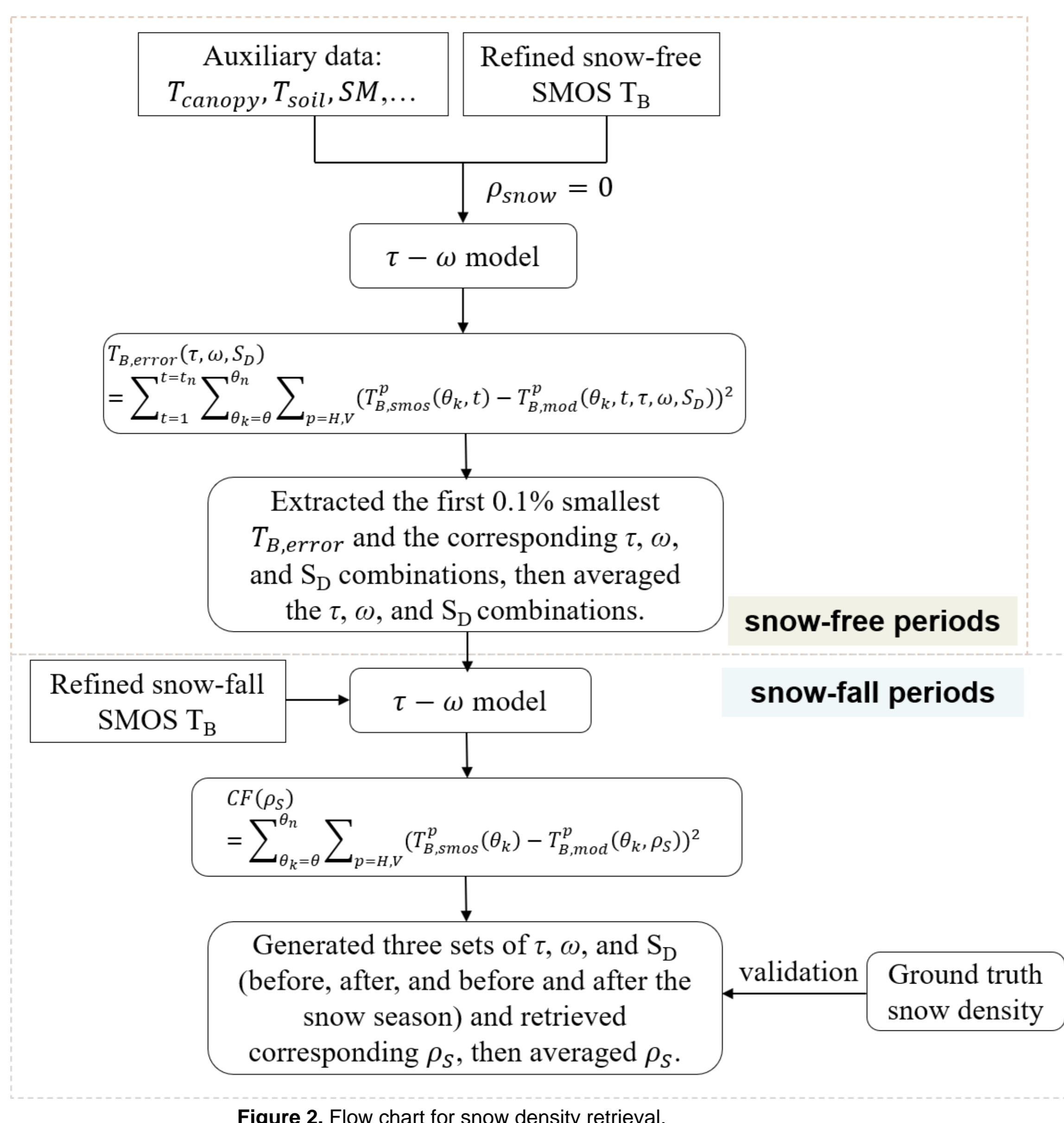


Figure 2. Flow chart for snow density retrieval.

Results

Performance of Multiple-Angle T_B Simulation

Figure 3 shows that for the HQ-CM4E station, the simulated T_B matched well with the SMOS-observed T_B , except for large incidence angles at horizontal polarization and unstable snow conditions (Figure 3a). On 29 November 2019 (Figure 3a), the relatively low-biased T_B at small angles and the complex snow condition during this season resulted in an underestimation of snow density. However, in Figure 3b–f, the errors between the retrieved snow density and in-situ measurements were within 45 kg/m³.

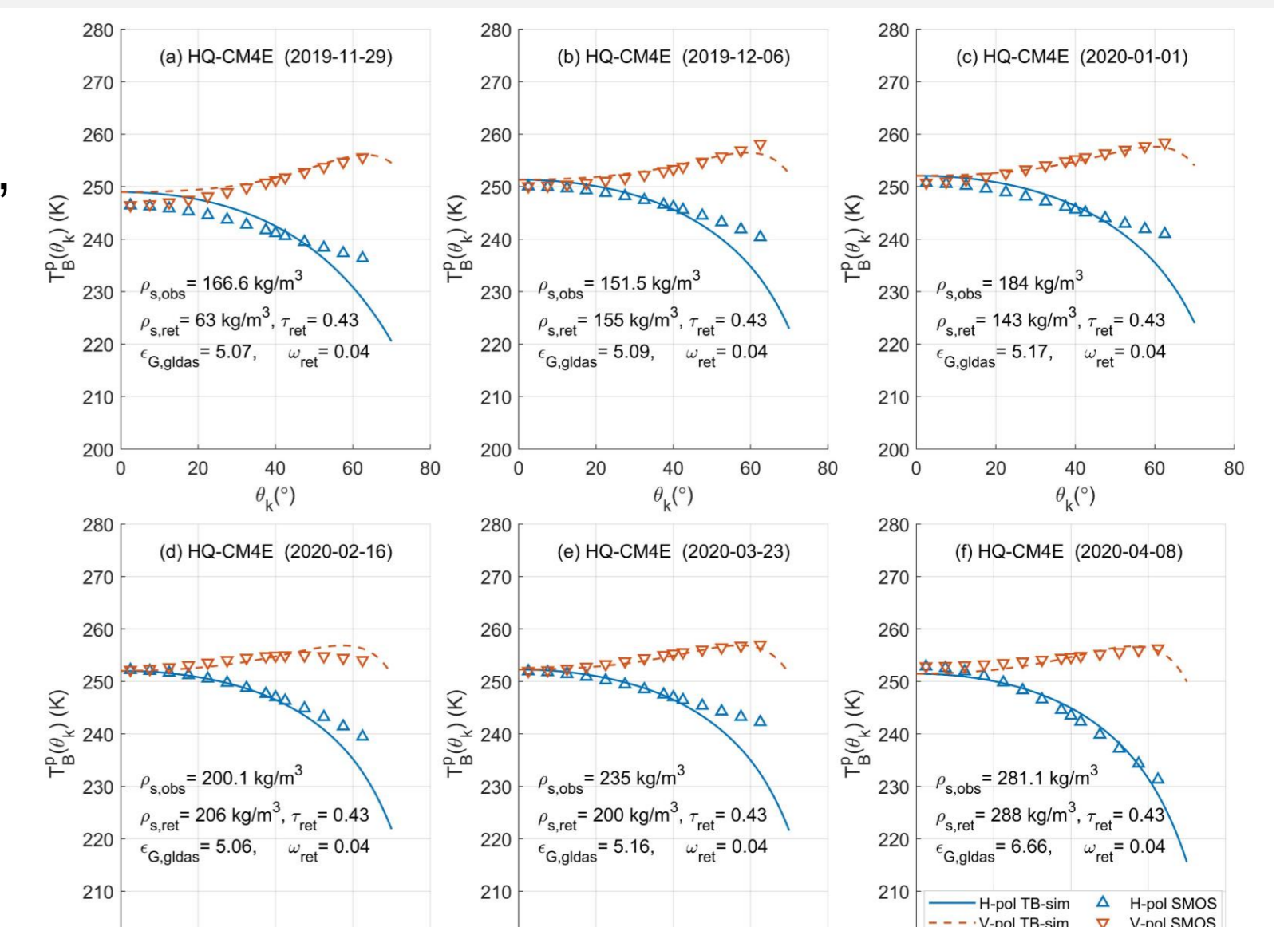


Figure 3. Examples of SMOS-observed T_B versus the forward-model-simulated T_B to fit the observations.

Performance of Snow Density Retrieval at Example Stations

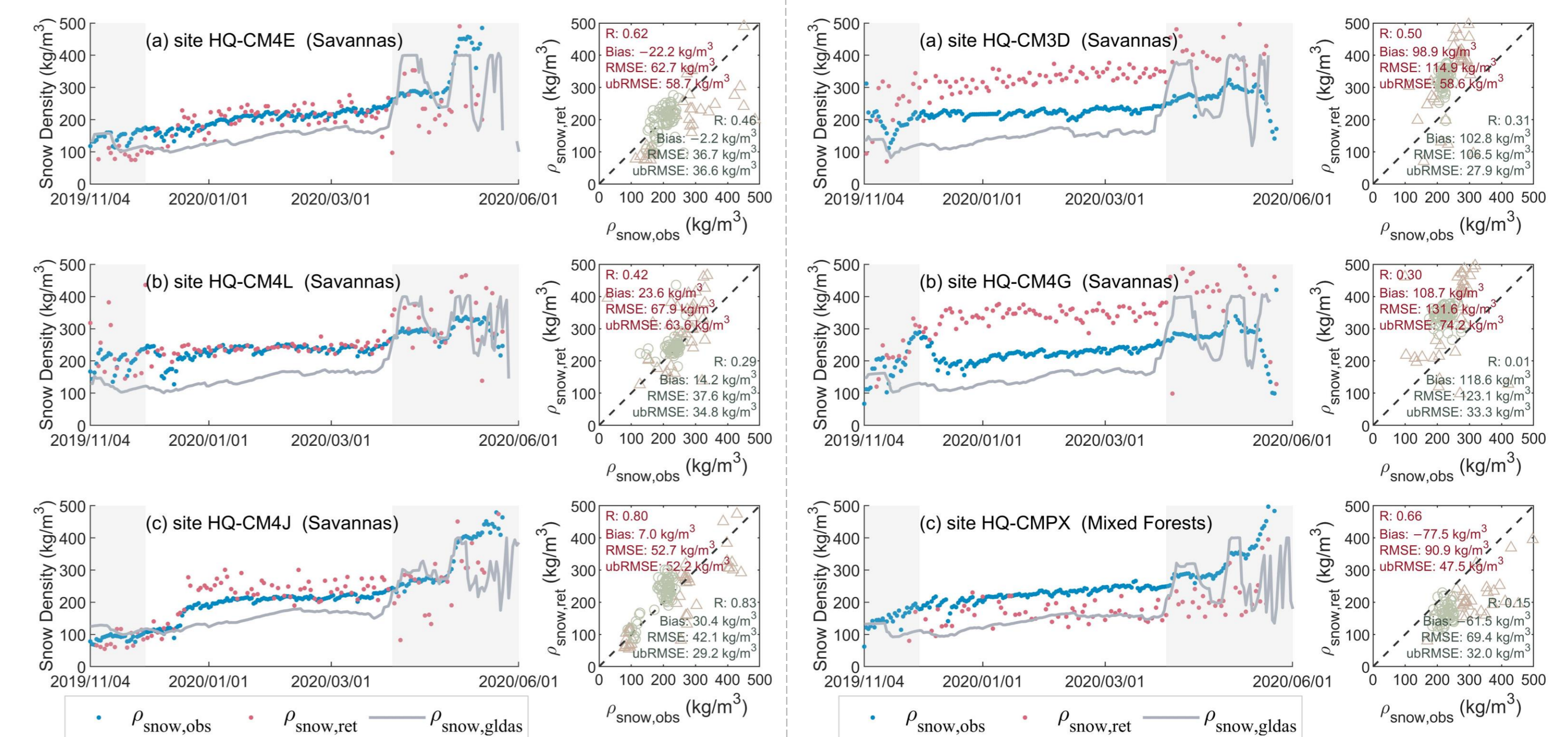


Figure 4. Time series and scatterplots of in-situ and retrieved snow density at the three: (a) HQ-CM4E, (b) HQ-CM4L, (c) HQ-CM4J.

Figure 5. Time series and scatterplots of in-situ and retrieved snow density at the three stations: (a) HQ-CM3D, (b) HQ-CM4G, (c) HQ-CMPX.

Validation of Retrieved Snow Density at All Stations

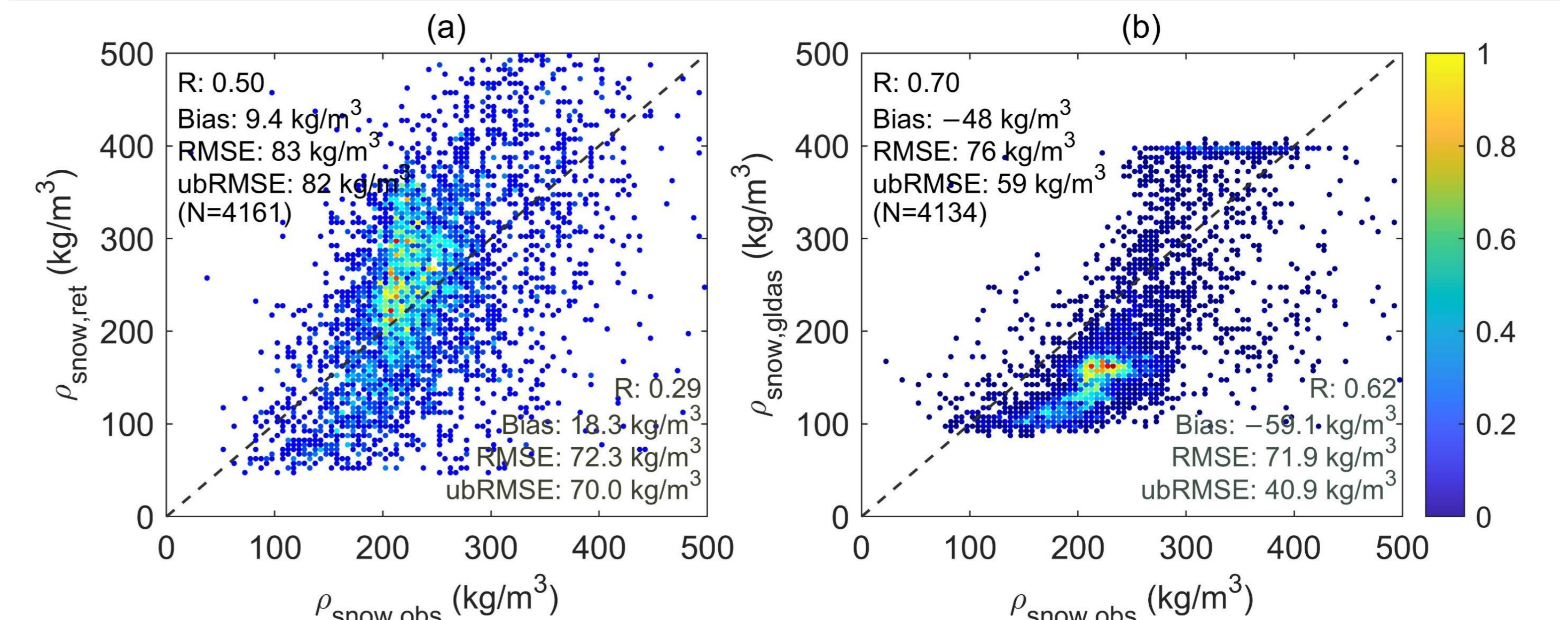


Figure 6. Scatterplots of (a) retrieved snow density and (b) reanalysis snow density from GLDAS against observed snow density from October, 2019 to June, 2020 at 43 stations located in Quebec, Canada.

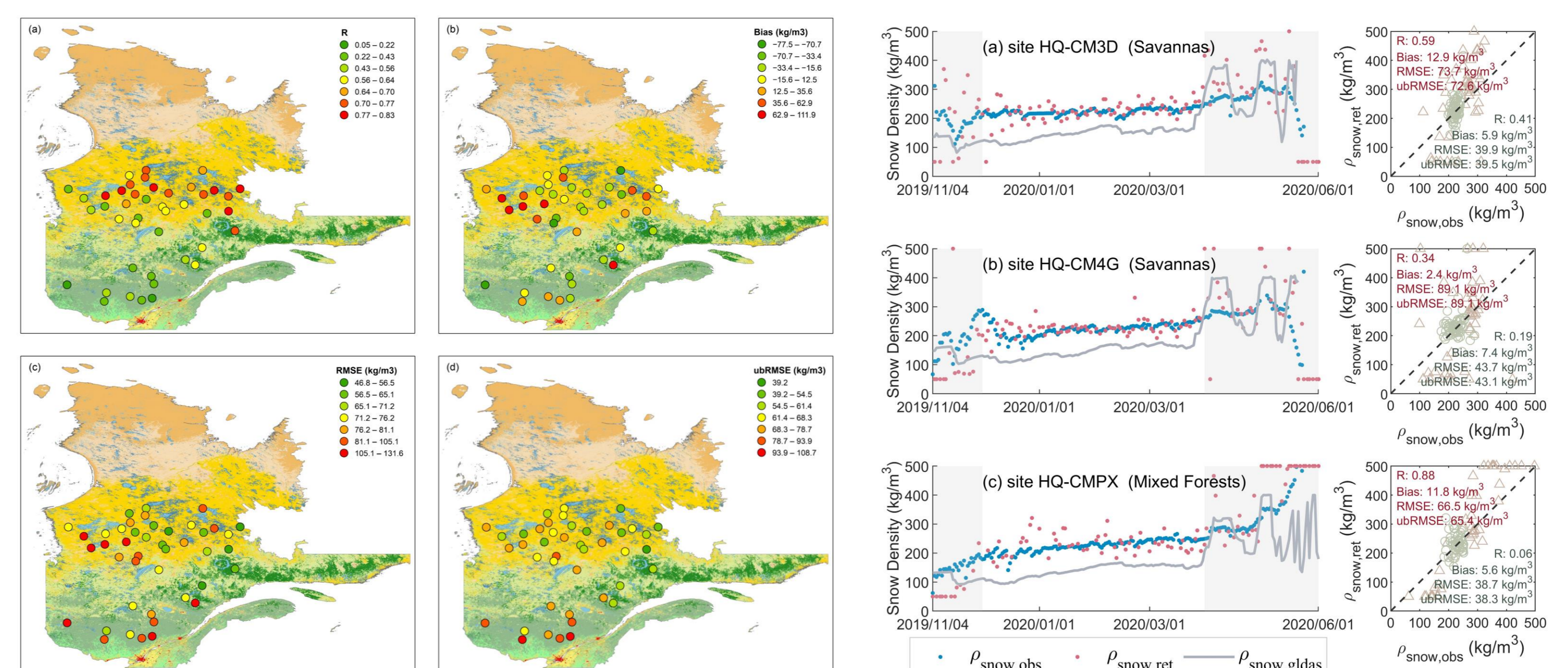


Figure 7. Distribution of R, mean Bias, RMSE, and ubRMSE of retrieved snow density at stations on map.

Figure 8. Time series and scatterplots of in-situ and retrieved snow density using manually adjusted predetermined parameters (τ , ω , S_D) at the three stations: (a) HQ-CM3D, (b) HQ-CM4G, (c) HQ-CMPX.

Table 1. The validation metrics of retrieved snow density compared with in-situ measurements summarized based on the MCD12Q1 IGBP classification.

MCD12Q1 IGBP Classification	R	Bias (kg/m ³)	RMSE (kg/m ³)	ubRMSE (kg/m ³)	Station Number
evergreen needleleaf forest	0.35	-33.44	78.55	71.08	1
woody savannas	0.55	-16.81	85.81	84.15	4
mixed forest	0.47	12.5	76.59	75.56	10
savannas	0.5	-11.37	82.8	82.01	28
ALL SITES	0.5	9.44	82.89	82.35	43

Conclusion

This study conducted snow density retrieval experiments based on L-band multiple-angle SMOS satellite observations and compared the results with the in-situ measurements from 43 CanSWE stations in Quebec, Canada. A forward model was used to describe the emission of the soil–snow–vegetation system. The vegetation and soil roughness parameters were objectively determined using SMOS T_B in the snow-free period and applied to estimate the snow density. The new retrieval method achieved bias of 9.4 kg/m³ and an RMSE of 83 kg/m³ for snow density at all stations. Currently, some stations show large systematic biases, but these biases can be reduced.